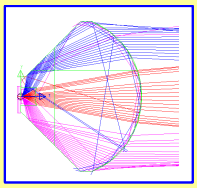

Ventura Photonics

Photonics Solutions

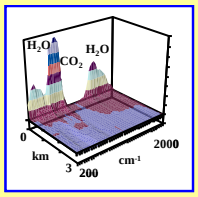

Dynamic Climate Energy Transfer and the Second Law of Thermodynamics

Roy Clark PhD

Ventura Photonics Climate Note 7, VPCN 007.1
Ventura Photonics
Thousand Oaks, CA
September 2019

Summary

The Earth and the Moon are located at similar distances from the sun. However, their surface temperatures are very different. This is because the Earth has an atmosphere and oceans whereas the surface of the Moon is mainly regolith with almost no atmosphere. The axial rotation of the Earth and the Moon produce a time dependent solar flux at the surface. The moon is in approximate thermal equilibrium with the solar flux. There is almost no time delay or phase shift between the change in solar flux and the surface temperature response. On the Earth, the diurnal time delay can easily reach 2 hours and the seasonal delay may reach 6 to 8 weeks. This means that the Earth stores and releases the absorbed solar heat over a wide range of time scales. There is no thermal equilibrium. The concept of an 'equilibrium average climate' controlled by a balance between the 24 hour average absorbed solar flux and the average long wave IR (LWIR) flux returned to space is invalid. The radiative convective equilibrium assumption that underlies the climate models used today has no basis in physical reality. 'Global warming' is nothing more than a mathematical artifact produce by the simplifying assumptions used to construct the basic climate models. The surface temperature of the Earth is set by a subtle balance between the time dependent heating and cooling flux terms coupled to a set of thermal reservoirs. A change in surface temperature requires a change in heat content or enthalpy of the local surface thermal reservoir divided by the heat capacity. In order to transfer heat between thermal reservoirs a thermal gradient is required. For evaporation, a humidity gradient is required, which generally includes a thermal gradient to establish the required difference in water vapor pressure. The Earth's climate is determined by the Second Law of Thermodynamics, not the First.

Introduction

The Earth and its moon are isolated planetary bodies that are heated by electromagnetic radiation from the sun and cooled by net long wave IR (LWIR) emission back to space. However, the Earth has oceans and an atmosphere, while the moon's surface is mainly regolith, a layer of rock derived soil with almost no atmosphere. In addition, the period of rotation of the Earth is 24 hours while that of the moon is 28 days. The moon is in approximate thermal equilibrium with the solar flux. This means that the daytime surface temperature is sufficient to dissipate the absorbed solar flux as LWIR emission without any significant time delay or phase shift between the absorption and emission. On Earth, the surface energy transfer processes include convection or sensible heat flux and evaporation or latent heat flux as well as LWIR emission. The energy transfer processes at the land-air and ocean-air interfaces are different and have to be considered separately. There is no thermal equilibrium. As the surface warms, the combined rate of cooling from net LWIR emission and moist convection lags the rate of heating. Over land, under clear sky conditions, the peak surface temperature may not be reached until 2 hours or more after local solar noon. Over the oceans, the seasonal phase shift between summer solstice and peak ocean surface temperatures may reach 6 to 8 weeks [Clark, 2019a].

In order to simplify the description of the surface energy transfer it is often assumed that the Earth is in thermal equilibrium between a '24 hour average absorbed solar flux' and an 'average emitted LWIR flux' [Arrhenius, 1896; Manabe and Wetherald, 1967]. An approximate energy balance is required by the First Law of Thermodynamics. However, this simply means that the surface temperature has to be maintained within the fairly narrow bounds needed to sustain life. It does not lead to any requirement for an exact flux balance. The requirement for climate stability comes from the Second Law of Thermodynamics, not the First. The local thermal gradient at the surface-air interface must be sufficient to dissipate the absorbed solar flux. The time dependence must be included. The various flux terms are coupled to a surface thermal reservoir. The absorbed solar heat is stored and released over a wide range of time scales. For the oceans, transport effects must also be included. Any change in surface temperature is determined by the change in heat content or enthalpy of the local thermal reservoir divided by the heat capacity. The LWIR flux cannot be separated and analyzed independently of the other flux terms. Unfortunately, the climate models used to 'predict' global warming are based on the convective radiative equilibrium assumption. Physical reality has been abandoned in favor of mathematical simplicity. The climate models must fail before any computer code is even written [Clark, 2019b; 2019c].

The concept of an average planetary energy balance also leads to an incorrect description of the so called 'greenhouse effect' in terms of mathematical averages with little useful physical meaning [Taylor, 2006]. The solar flux at the top of the atmosphere (TOA) is near 1366 ±45 W m^{-2}. The values selected depend on satellite radiometer calibration [Wilson, 2014]. The Earth's average albedo or reflectivity is near 0.3. This means that an average absorbed solar flux is approximately 956 W m^{-2}. The geometry is that of a sphere illuminated by a disk of almost collimated radiation. The area ratio of a sphere to a circular disk of the same radius is 4. The average emitted LWIR flux over the entire Earth should therefore be near 240 W m^{-2}. This is close to average values

derived from satellite observations [Loeb et al, 2009]. Using Stefan's law, the average flux may be converted to an 'effective emission temperature' of 255 K (-18 C). The Earth's 'average surface temperature' is near 288 K (15 C). This leads to the idea that the Earth is 33 C warmer that it would be without any IR 'absorption and emission' in the atmosphere. This temperature difference is often called the 'greenhouse effect temperature'.

In reality, there is no equilibrium, no average surface temperature and no simple greenhouse effect temperature increase. The spectral distribution of the LWIR emission to space is certainly not that of a blackbody at 255 K. In addition, the local value of this LWIR flux may easily vary from 150 to 350 W m^{-2}. Instead, the TOA LWIR flux has to be interpreted as the cumulative cooling flux emitted by many different levels of the atmosphere at different temperatures [Clark, 2019d; Feldman et al, 2008]. The upward and downward LWIR fluxes through the atmosphere are decoupled by molecular line broadening effects. Almost all of the downward LWIR flux from the lower troposphere to the surface originates from within the first 2 km layer above the surface. This establishes an exchange energy with the upward blackbody emission from the surface which limits the net LWIR cooling flux that can be emitted by the surface. In order to dissipate the absorbed solar heat, the surface must warm up until the excess heat is removed by moist convection. This is a mass transport process. The ascending air parcel must perform mechanical work to overcome the Earth's gravitational potential. This sets the local lapse rate or temperature profile of the troposphere. In addition, the rising air is coupled to the angular momentum or rotation of the Earth. This establishes the Hadley, Ferrell, Polar convective cell structure and the trade winds that drive the ocean gyre circulation. These in turn determine the Earth's basic weather patterns. The greenhouse effect has to be explained through the application of the Second Law of Thermodynamics to the time dependent surface exchange energy.

The role of the Second Law of Thermodynamics in setting the surface temperature will now be examined in more detail. First, the surface temperature of the Moon is described using a simple radiative heat transfer balance. Then the more complex case of the Earth is considered. This involves five different energy transfer processes.

1) The LWIR surface exchange energy limits the net LWIR surface cooling.

2) Over land, all of the flux terms are coupled to a thin surface layer. The absorbed solar heat establishes thermal gradients both between the surface and the air above and between the surface and the subsurface layers below. The excess solar heat is removed by moist convection. The subsurface heat transfer is localized to the first few meters and almost all of the absorbed heat is returned to the troposphere during the same diurnal cycle. The diurnal phase shift may reach 2 hours and there is no direct seasonal phase shift. The heat capacity of the land thermal reservoir is too small.

3) Over the oceans, the surface is almost transparent to the solar flux. Water does not act as a blackbody absorber for the solar flux. Approximately 90% of this flux is initially absorbed into the first 10 m layer of the ocean. The heat capacity of this layer limits the ocean temperature rise.

The thermal gradient at the ocean-air interface is small, typically 1 or 2 K. This means that the bulk ocean must warm up until the surface temperature is sufficient for the water vapor pressure to support the removal of the excess solar heat by wind driven evaporation. The absorbed solar heat is then mixed into first 100 m layer of the ocean by convection. There is a seasonal phase shift that may reach 6 to 8 weeks between the peak solar flux at solstice and the peak surface temperature response.

4) Wind coupling at the ocean surface establishes the ocean gyre circulation that transports the absorbed solar heat over long distances and leads to the formation of the equatorial warm pools. There is never an exact flux balance between the absorbed solar flux and the wind driven evaporation. This leads to the development of the ocean oscillations.

5) The interaction between the convection and the rotation or angular momentum of the Earth creates the basic weather patterns, particularly the mid latitude cyclone/anticyclone systems. The large heat capacity of the air isolated within these systems stores the basic information of the ocean surface temperature during weather system formation. As these weather systems move over land, the ocean temperature is retained as the night time convection transition temperature. This is the mechanism of climate change that couples the changes in surface ocean temperature to the land surface temperature.

The energy transfer processes at the land-air and ocean-air interfaces are illustrated in Figure 1.

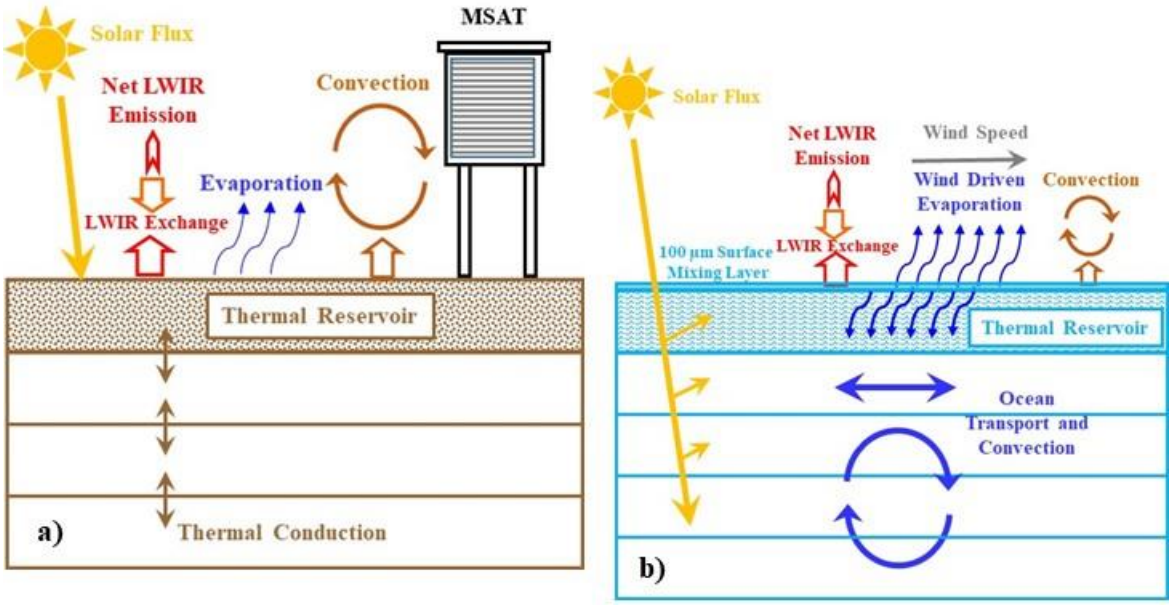

Figure 1: Energy transfer processes at the land-air and ocean-air interfaces (schematic)

The various thermal and humidity gradients at the surface dissipate the surface heat. The troposphere then transports this heat to the middle to upper troposphere by moist convection. From here it is radiated to space. At minimum, the troposphere has to be described in terms of four coupled thermal reservoirs that function together as an open cycle heat engine [Clark, 2013a;

2013b]. The land and especially the oceans are the hot reservoirs ('boilers') of this engine. The downward LWIR flux to the surface and the outgoing LWIR radiation to space are decoupled by molecular line broadening effects. The troposphere therefore divides naturally into two independent thermal reservoirs. Almost all of the downward LWIR flux reaching the surface originates from within the first 2 km layer that forms the lower tropospheric reservoir. The LWIR emission to space originates mainly from the upper tropospheric reservoir that extends from 2 km to the tropopause. This acts as the cold reservoir of the heat engine. The heat lost by LWIR emission to space is replaced by convection from below. Above the tropopause, the stratosphere forms another independent thermal reservoir. The main heat source here is absorption of the UV solar flux by ozone and the cooling is dominated by LWIR emission from CO_2.

The Surface Temperature of the Moon

The moon is illuminated by the full solar flux, without any atmospheric attenuation. At the surface, the incident flux varies with the cosine of the zenith angle. The absorbed solar flux depends on the surface absorption coefficient and surface reflectivity, which also depends on the solar zenith angle. The surface temperature may be estimated using:

$$T = (I_A/(\sigma\varepsilon))^{0.25} \quad (1)$$

$$I_A = I_0 \alpha R_{\theta z} \cos\theta_z \quad (2)$$

where I_A is the absorbed solar flux, σ is Stefan's constant, ε is the IR emission coefficient, α is the solar absorption coefficient, $R_{\theta z}$ is the angle dependent surface reflectivity and θ_z is the zenith angle. The surface temperature of the moon at the equator is shown in Figure 2a [Volokin and ReLlez, 2014]. Figure 2b shows the surface temperature from the first 6 lunar hours in Figure 1a with the temperature calculated from Eqns. 1 and 2 superimposed (blue line). Here ε is set to 0.95, α to 0.9 and $R_{\theta z}$ is the Fresnel reflection calculated for a refractive index of 1.5. Thermal storage within the regolith layer has not been included. One lunar hour is 27.3 Earth hours. The calculated temperature is in good agreement with the measured one.

During the day, the absorbed solar flux is converted to LWIR emission and radiated back to space with almost no time delay or phase shift. At night, the surface cools slowly from 125 to 93 K by LWIR emission as stored solar heat is removed from the regolith. The night time LWIR cooling fluxes are from approximately 14 to 4 W m^{-2}. The thermal gradient is the temperature difference between the lunar surface and that of outer space. The concept of an average surface temperature is not a very useful one. The diurnal temperature change is 296 K. There are also issues with the temperature averaging process related to Hölders inequality. The average temperature derived directly from the surface temperature is different from that derived from the average flux. Lunar temperatures are discussed in detail by Volokin and ReLlez [2014].

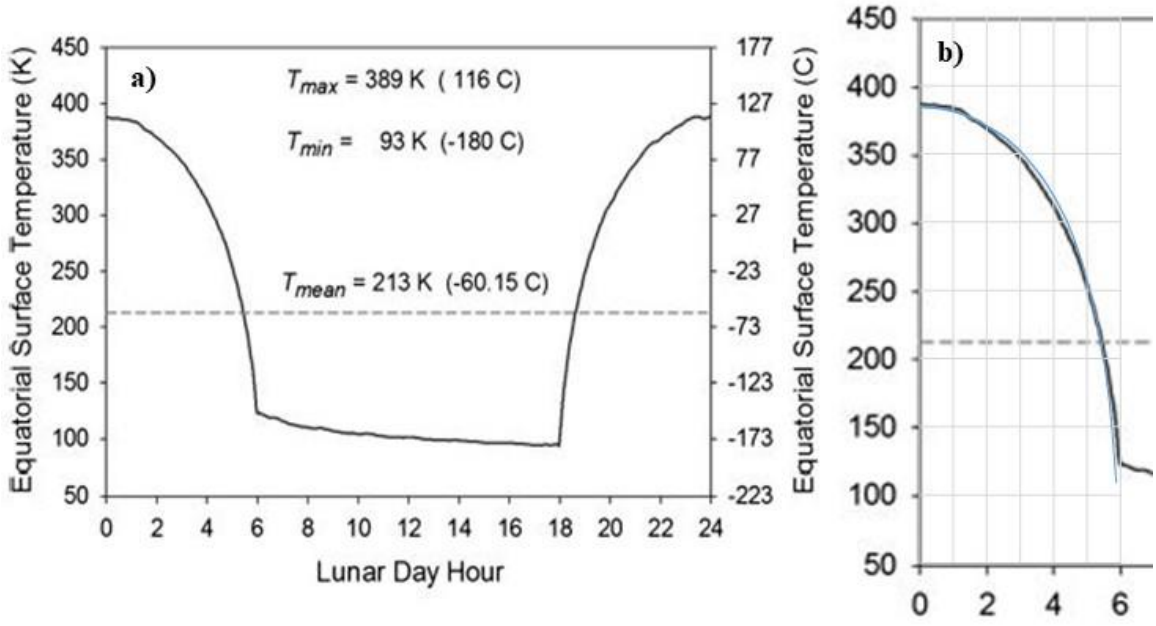

Figure 2: a) Diurnal temperature variation of the moon's surface at the equator and b) comparison with temperature calculated from Eqns. 1 and 2 shown as blue line.

The Surface Temperature of the Earth

1) The Surface Exchange Energy

The presence of so called greenhouse gases in the atmosphere adds a downward LWIR flux from the lower troposphere to the surface. This establishes an exchange energy that limits the net LWIR emission from the surface. Figure 3 shows the results from a MODTRAN simulation of the downward LWIR flux reaching the surface. The surface and air temperatures are set to 300 K. The spectral resolution is 2 cm^{-1} and the spectral range is from 100 to 1500 cm^{-1}. The CO_2 concentration is 400 ppm and the surface relative humidity is 0.7 with the tropical atmosphere option [MODTRAN, 2018]. The upward blackbody emission from the surface in the 100 to 1500 cm^{-1} spectral range is 419 W m^{-2} of which 328 W m^{-2} is blocked by the exchange energy and 91 W m^{-2} is transmitted into the atmospheric window. The downward emission from within the H_2O and CO_2 absorption bands acts as a blackbody because of the molecular line pressure broadening.

When the surface is warmer than the air above, the exchange energy still blocks most of the LWIR emission from the surface. The net LWIR flux through the LWIR transmission window increases. However, the rest of the additional surface LWIR flux is absorbed mainly by the H_2O and CO_2 bands. This absorbed heat adds to the convective flow from the surface. The calculation of the exchange energy requires a detailed radiative transfer analysis. However, this may be simplified to the difference in blackbody emission at the surface and air temperatures with an additional LWIR flux term to account for the effect of the atmospheric LWIR transmission window.

$$\Delta Q_{irnet} = \sigma(\varepsilon T_s^4 - T_a^4) + \Delta Q_{irwin} \quad (3)$$

where σ is Stefan's constant, ε is the surface emissivity, T_s is the surface temperature, T_a is the surface air temperature and ΔQ_{irwin} is the LWIR transmission window loss. There are two different thermal gradients associated with Eqn. 3. The first is the difference in bulk temperature between the surface and the air above. Here, T_a is set to the MSAT temperature. The second is the effective temperature of the downward LWIR emission to the surface in the LWIR transmission window [Clark, 2019a].

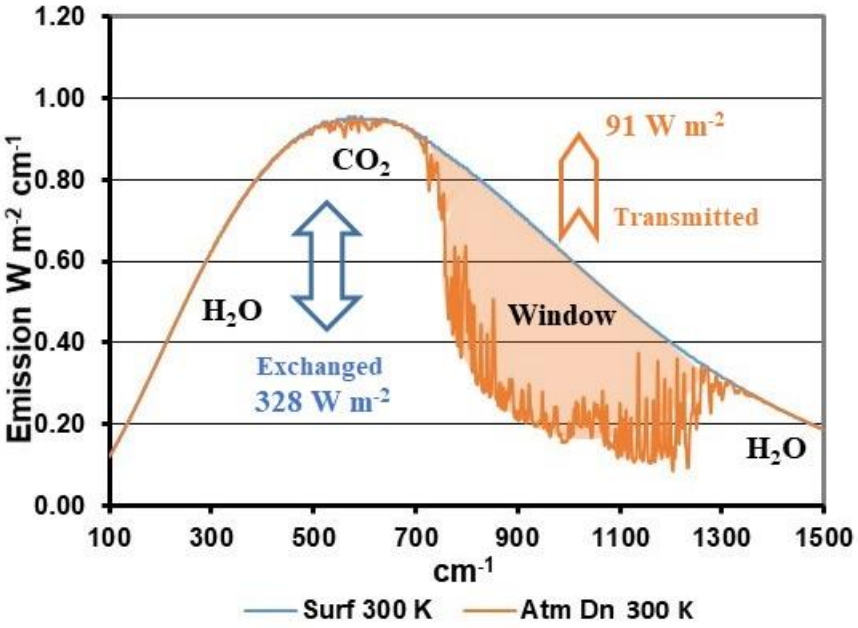

Figure 3: Surface exchange energy and the LWIR transmission window (MODTRAN calculation).

2) The Land Surface Temperature

The net LWIR cooling flux is insufficient to dissipate the absorbed solar heat from the surface. As the surface warms, heat is transferred directly from the surface to the adjacent air molecules. The warm air expands, it becomes buoyant and transports the heat upwards away from the surface. This establishes a convective flow from the surface. The warm air that rises is replaced by cooler air from above. Over land, as the surface warms during the day, a thermal gradient is also established between the surface and the subsurface layers below. Heat is conducted and stored below the surface. Later in the day, this stored heat is returned to the surface as the subsurface thermal gradient reverses. These energy transfer processes for a dry land surface are illustrated in Figure 4. The various flux terms are shown in Figure 4a. There is a delay of approximately 2 hours between the peak solar flux at local noon and the peak net LWIR and convection fluxes. The maximum heat flux conducted below the surface occurs about an hour before local noon and the heat flow reverses during the afternoon. Convection is a complex turbulent mixing process. The convective surface cooling or sensible heat flux is often simplified by using a single convection coefficient k_{conv} and the bulk surface - air temperature difference.

$$\Delta Q_{sens} = k_{conv}(T_s - T_a) \quad (4)$$

Over dry land, k_{conv} is approximately 15 to 20 W m^{-2} K^{-1} [Clark, 2011]. Over the oceans it is near 5 W m^{-2} K^{-1} [Sahlee et al, 2008]. Here, the air temperature is taken as the MSAT temperature. Definitions may vary in the literature.

The surface and the air or MSAT temperatures are shown in Figure 4b. It is important to note that the weather station temperature is the meteorological surface air temperature (MSAT) measured in a ventilated enclosure located at eye level, 1.5 to 2 m above the ground [Oke, 2006]. In this example, the surface temperature reaches 50 C while the MSAT temperature only reaches 25 C. The peak temperature is reached 1 to 2 hours after the noon solar flux peak. During the evening, the surface and air temperatures cool until they approach the same temperature.

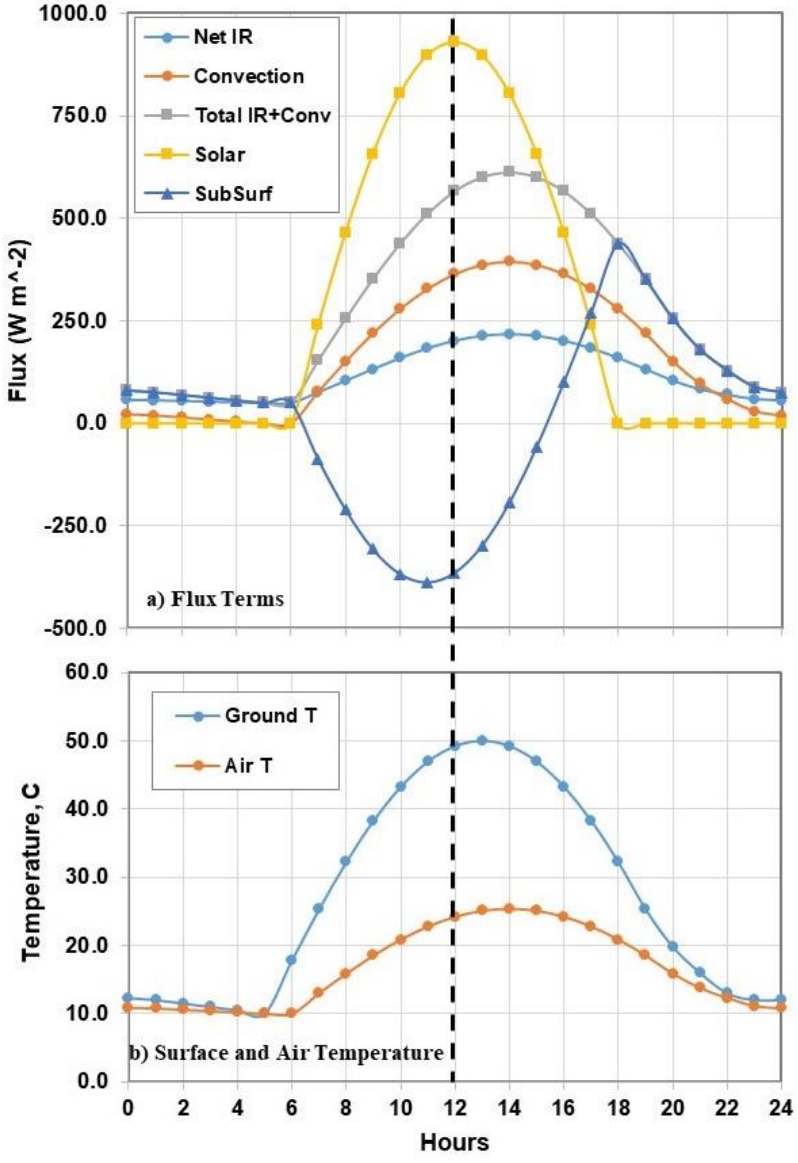

Figure 4: a) flux terms and b) surface and air temperatures for a dry surface under full summer sun illumination.

If the surface is moist, it will also cool by water evaporation that is coupled to the convective flux. This reduces the surface temperature rise. Over land, the detailed description of the surface evaporation (evapotranspiration) is complex [Mengelkamp et al, 2006]. The latent heat flux usually peaks during the middle of the day and decreases significantly at night. However, the flux may also be limited by the transport of subsurface moisture to the surface.

Another important concept is the night time convection transition temperature. As the land surface cools in the evening, the surface and surface air temperatures equalize and convection essentially stops. The surface now cools more slowly by net LWIR emission through the LWIR transmission window until the solar heating cycle starts the next day. The convection transition temperature is reset each day by local weather system [Clark, 2019a].

3) The Ocean Surface Temperature

The energy transfer processes at the ocean-air interface are quite different from those at the land-air interface. The ocean surface is almost transparent to the solar flux. Approximately half of the incident solar radiation is absorbed within the first 1 m layer of the ocean and 90% is absorbed within the first 10 m. The thermal gradient at the surface is generally small, 1 or 2 K. Under these conditions, the ocean surface warms until the excess solar heat is dissipated by wind driven evaporation. Following Yu [2007], the latent heat flux ΔQ_{lat} is given by

$$\Delta Q_{lat} = k_{lat}(P_{Tws} - R_h P_{Twa})U \qquad \text{(Eq. 4)}$$

Where P_{Tws} is the vapor pressure at the water surface temperature T_{ws}, P_{Twa} is the vapor pressure at the surface air temperature, T_{wa}, R_h, is the relative humidity, U is the wind speed and k_{lat} is an empirical constant.

The cooler water produced at the surface then sinks and cools the bulk ocean layers below. It is replaced by upwelling warm water. This is a Rayleigh-Benard type of convection with columns of water moving in opposite directions. It is not a simple diffusion process. This convection cycle continues to provide heat to the surface at night, so the wind driven evaporation continues at night. The thermal storage is not localized and heat can be transported and recirculated over very long distances.

There is a diurnal phase shift between the solar flux and the ocean surface temperature rise that depends on both the solar flux and the wind speed. Figure 5 shows the effect of wind speed on the diurnal temperature rise recorded at the TRITON buoy located on the equator at a longitude of 165° E in the Pacific warm pool. These data were recorded during July 2010 [NOAA, TAO, 2012].

During the summer at most latitudes, the solar heating exceeds the wind driven cooling. The lower subsurface layers are not coupled to the surface by convective mixing and a stable thermal gradient is established. During the winter, the wind driven evaporation exceeds the solar heating and the surface temperatures cool and establish a uniform temperature layer down to 100 m or below.

There is a significant time delay or phase shift of 4 to 8 weeks between the solstice and the ocean max/min temperature response. Figure 6 shows the seasonal variation in ocean temperature at nominal depths of 5, 25, 50, 75 and 100 m derived from Argo float data [Clark, 2013a, 2013b; 2011]. Figure 6a shows the temperature data from a float drifting in the S. Pacific Ocean at latitudes and longitudes near 21° S and 105° W. Higher latitudes show a similar behavior with lower temperatures because of reduced solar heating.

At low latitudes near the equator, the diurnal and seasonal temperature variations may not be sufficient to mix the subsurface layers below the 25 to 50 m levels and heat can accumulate at these depths for extended periods. Figure 6b shows the temperature data from an Argo float drifting in the S. Pacific Ocean at latitudes and longitudes near 1.5° S and 126° W. The diurnal mixing layer is shallow and only extends down to the 50 m level about half of the time. The floats are not tethered and the decrease in near-surface temperature with time is caused by an eastward drift.

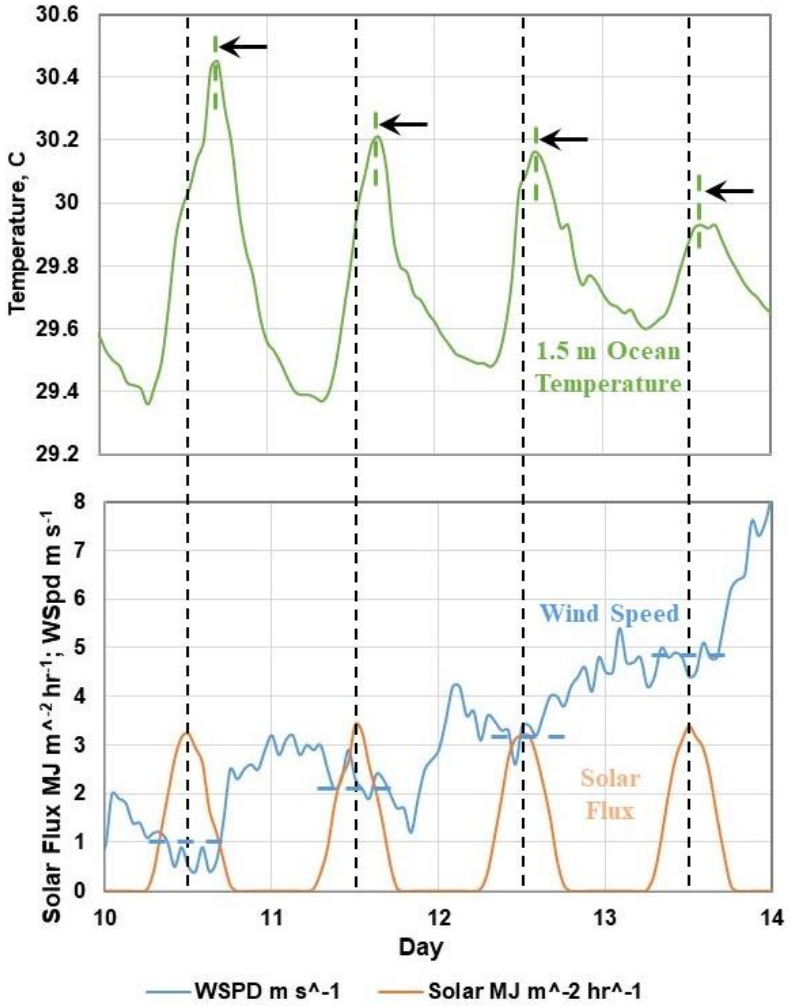

Figure 5: 1.5 m ocean temperature, wind speed and solar flux for 4 days, July 2010 recorded at the TRITON buoy on the equator at 165 E in the Pacific warm pool. The diurnal temperature rise and the magnitude of the phase shift decrease with increasing wind speed.

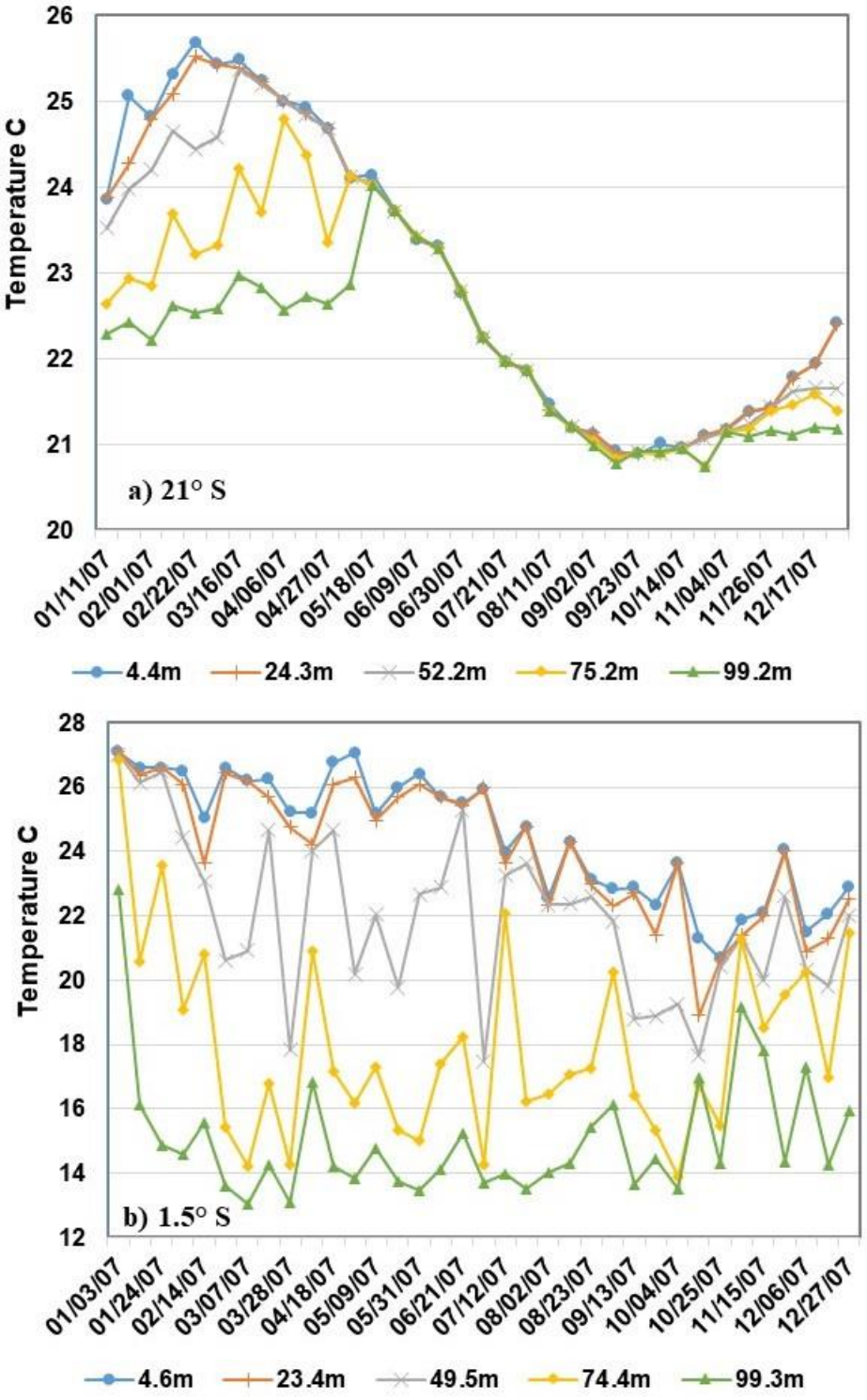

Figure 6: Argo float data for average latitudes of 21° and 1.5° S. At 21 S and higher latitudes, the solar heating and wind driven evaporation interact to produce a stable subsurface thermal gradient in the summer that is removed by excess cooling during the winter. Near the equator, the solar heating exceeds the evaporation in the eastern Pacific Ocean leading to the formation of the western equatorial warm pool.

4) Gyre Circulation, Equatorial Warm Pool Formation and Ocean oscillations

Heat continues to accumulate as the ocean water travels westwards with the Pacific equatorial current. This leads to the formation of the equatorial ocean warm pool in the western Pacific Ocean. The ocean surface temperature increases until the wind driven evaporation balances the tropical solar heating at a surface temperature near 30 C and an average wind speed near 5 m s^{-1}. The increase in ocean temperature across the equatorial Pacific Ocean derived from the TRITON buoy network is shown in Figure 7 [Clark, 2011].

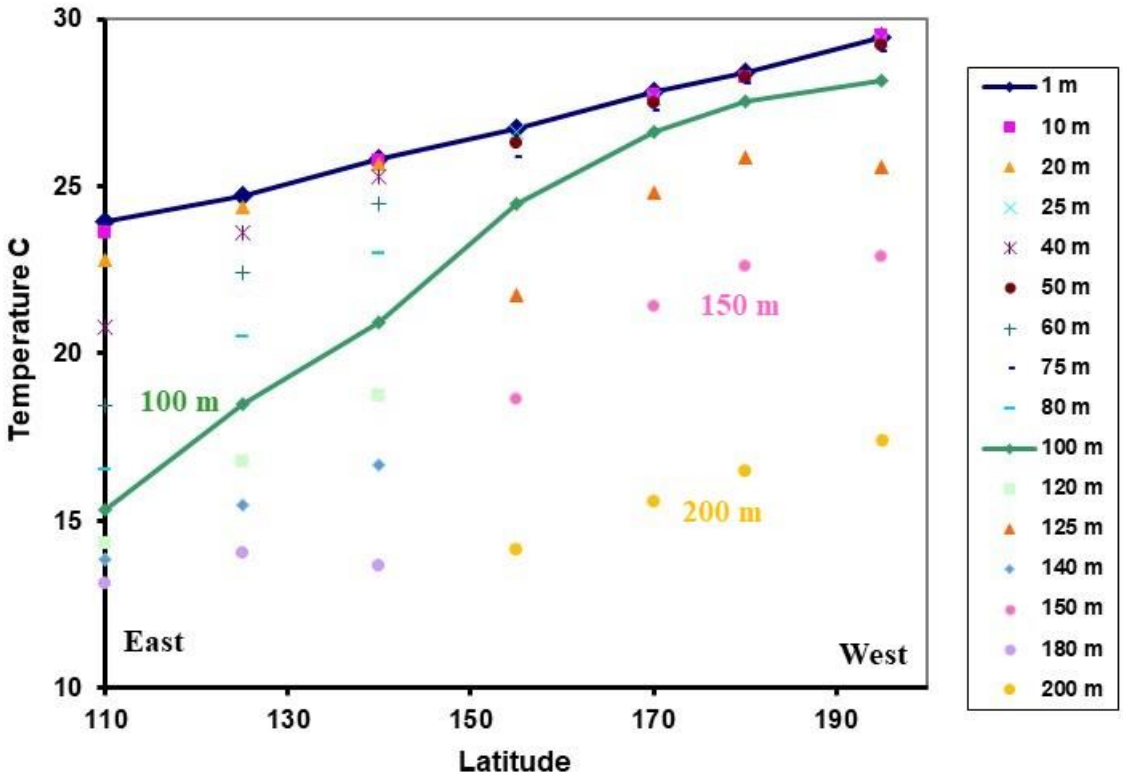

Figure 7: Formation of the equatorial pacific warm pool. Data from TRITON buoy network.

Variations in the wind speed across the Pacific Ocean then produce the characteristic ENSO oscillations. As the wind speed slows, the evaporation decreases and the ocean current velocity decreases. Both of these factors increase the rate of surface heating and the warm pool extent increases. The southern oscillation index (SOI) is the pressure difference between Tahiti and Darwin Australia. This a measure of the wind speed. There is an inverse relationship between the SOI and the ENSO. This is shown in Figure 8. For clarity, the sign of the SOI is inverted in the plot [ENSO, 2018; SOI, 2018].

The period of the ENSO varies between 3 and 7 years. In addition, there are longer term ocean oscillations such as the Pacific Decadal Oscillation (PDO) and the Atlantic Multi-decadal Oscillation (AMO) with periods near 60 to 70 years. It must be emphasized that these are quasi-

periodic oscillations that develop from the onset of instability in non-linear fluid dynamic systems. Analysis of the power spectrum of the AMO and PDO oscillations shows a strong peak near 9 years [Muller et al, 2013]. This means that caution is needed when attempts are made to link the ocean oscillations to solar, lunar or planetary cycles.

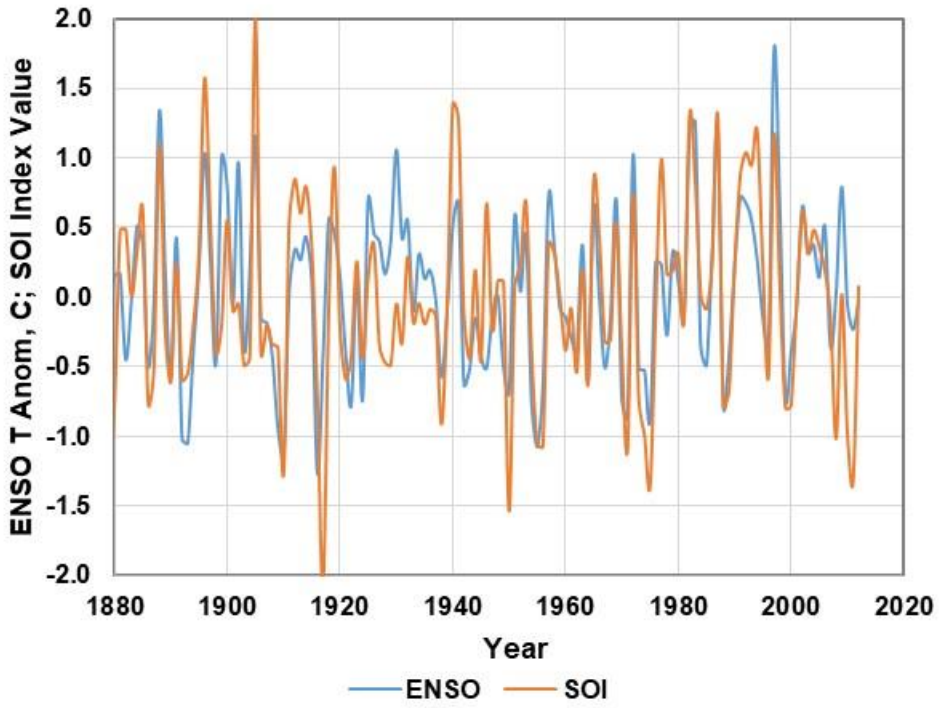

Figure 8: ENSO temperature anomaly and SOI index. For clarity, the SOI index is inverted (sign switched). This clearly shows that the ENSO is a wind driven oscillation that depends on the air pressure difference indicated by the SOI.

Part 5: Weather System Transport and the Convection Transition Temperature

Changes in ocean surface temperatures are coupled by weather system transport to weather stations that can be very far from the ocean. The coupling mechanism is the nighttime convection transition temperature. As the land surface and air temperatures cool in the evening, they both tend to equalize to the bulk air temperature of the local weather system passing through. This may be seen in the seasonal phase shift in the climate data of selected US weather stations near 34°, 45° and 20° latitudes. This is illustrated in Figure 9. A detailed description is given by Clark [2019a].

Another example of this coupling is the relationship between the surface temperature record and the AMO. This is shown in Figure 10. The influence of the AMO extends over large area of N. America, Europe and parts of Africa. The HadCRUT4 temperature series is an area weighted average of temperature anomalies derived from a 5° x 5° grid. The correlation coefficient between these two datasets is 0.8.

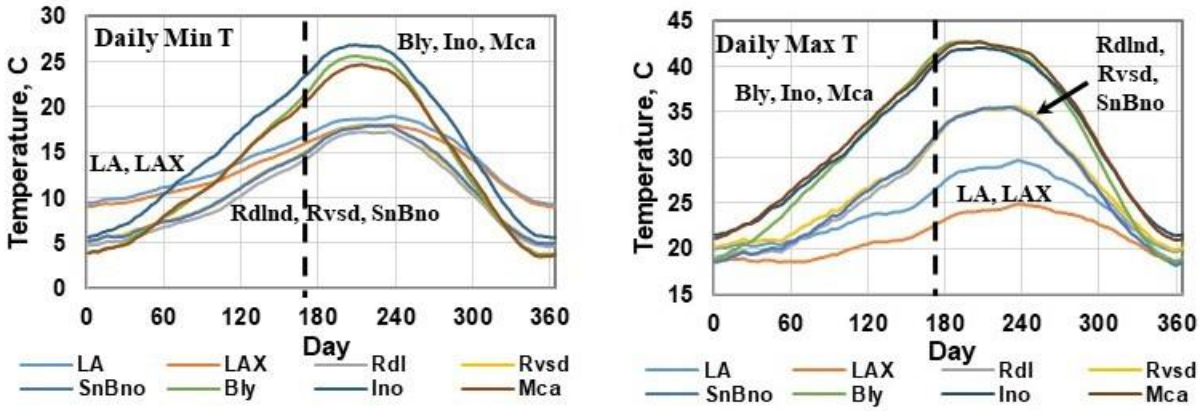

a) 34° Latitude, S. California Stations, Los Angeles, Los Angeles Airport, Redlands, Riverside, San Bernardino, Blythe, Indio, Mecca

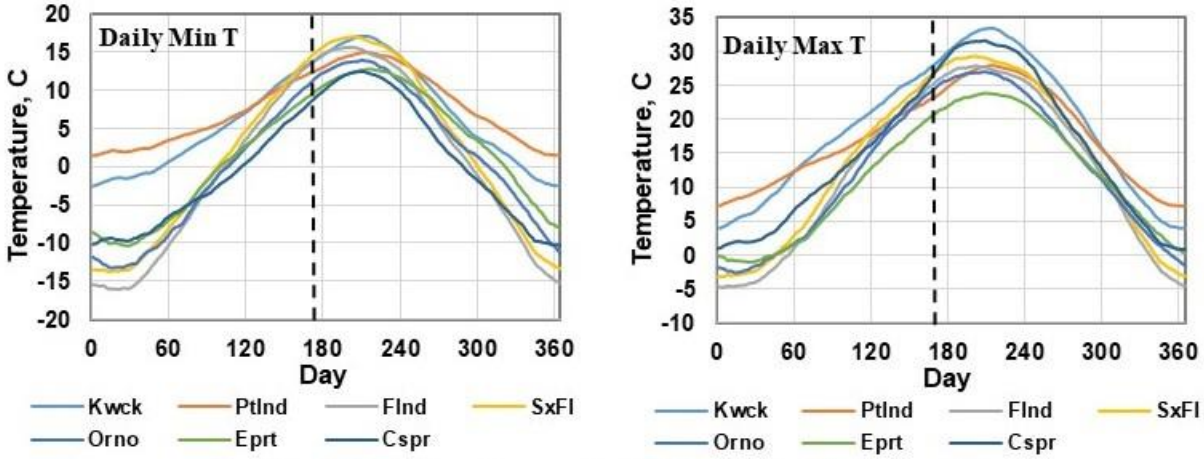

b) 45° latitude stations, Kennewick, WA, Portland, OR, Casper, WY, Flandreau and Sioux Falls, SD, and Orono and Eastport ME

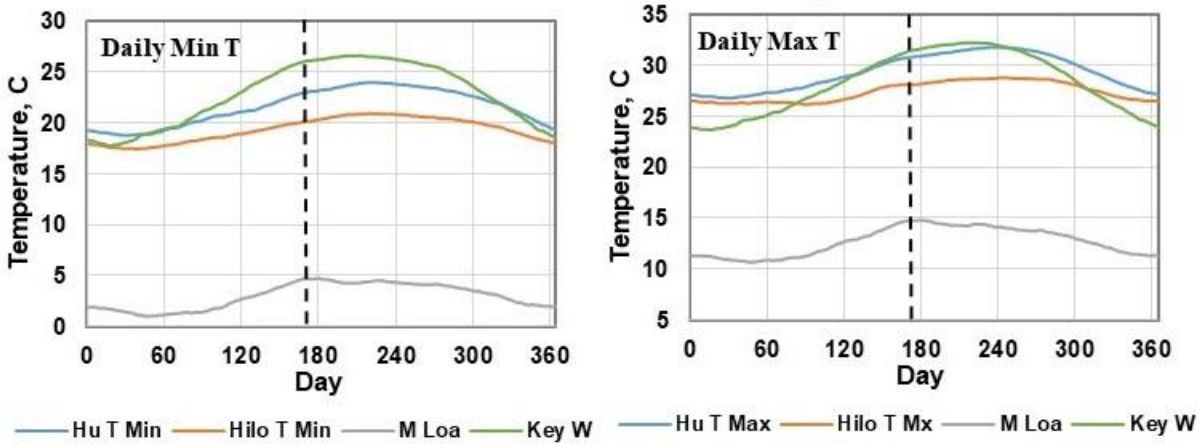

c) 20° latitude stations, Honolulu, HI, Hilo, HI, Mauna Loa, HI and Key West, FL.

Figure 9: 30 year minimum and maximum daily average temperatures for selected weather stations near 34°, 45° and 20° latitudes. The dotted lines indicated the peak solar flux at summer solstice. The seasonal phase shifts can be seen in the peak temperatures after solstice.

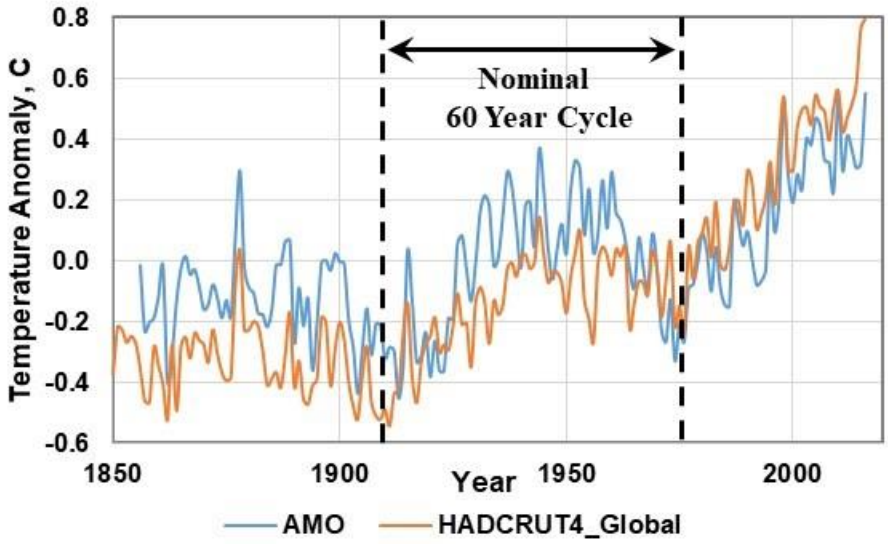

Figure 10: The AMO and the HadCRUT4 climate temperature series. These two are coupled by the convection transition temperature transported by the weather systems that form in region of the AMO. The correlation coefficient between these two data sets is 0.8.

The Effect of an Increase of a 2 W m^{-2} in Downward LWIR Flux on the Surface Temperature

Over the last 200 years, the atmospheric concentration of CO_2 has increased by about 120 ppm from 280 to 400 ppm [Keeling, 2019]. This has produced an increase of approximately 2 W m^{-2} in the downward LWIR flux from CO_2 reaching the surface [Clark, 2013a; 2013b; 2011; Harde. 2017]. Over the oceans, this small increase in flux is mixed with the wind driven evaporation in the surface layer and cannot penetrate below the surface. The penetration depth of the LWIR flux into water is less than 100 μm. The increase in wind speed needed to compensate for the ocean surface warming produced by a 2 W m^{-2} increase in LWIR flux is shown in Figure 11. This is based on a thermal engineering analysis of the ocean surface temperature discussed in detail by Clark [2019a, b]. The blue curve shows the increase in wind speed needed when a fixed LWIR window cooling flux of 45 W m^{-2} is used at all latitudes and reduced to 43 W m^{-2} to simulate the change in CO_2 LWIR flux. The orange curve shows the increase in wind speed using a temperature dependent LWIR window flux that increases by 2.2 W m^{-2} for each 1 C rise in surface temperature. The important point to note is that up to 30° latitude, the change in wind speed is below 10 CENTIMETERS per second. Typical variation in wind speed is 1 to 12 meters per second, with higher wind gusts. This is at least a factor of 10 to 100 larger than that needed to dissipate the 2 W m^{-2} LWIR flux from all of the increase in atmospheric CO_2 concentration over the last 200 years.

Over land, the 2 W m^{-2} increase in LWIR flux has to be added to the total flux balance. Most of the absorbed surface heat is dissipated by convection, not by the net LWIR cooling flux. For a bulk convection coupling coefficient of 20 W m^{-2} K^{-1}, this requires an increase in the surface thermal gradient of 0.1 K. This is too small to measure [Clark, 2019a].

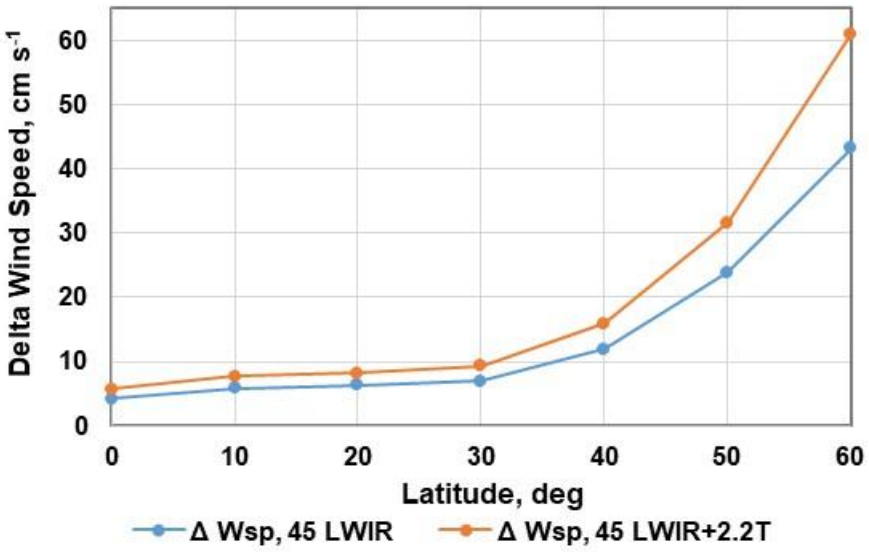

Figure 11: Change in wind speed (cm s^{-1}) needed to restore the ocean surface cooling flux when the downward LWIR flux is increased by 2 W m^{-2}. Both the fixed and the temperature dependent LWIR window flux cases are shown.

Conclusions

The surface temperature of the Earth may be understood through the application of the Second Law of Thermodynamics to the time dependent surface exchange energy. The downward LWIR flux from the lower troposphere exchanges photons with the blackbody emission from the surface. This reduces the net LWIR cooling from the surface. This is the real source of the so called 'greenhouse effect'. Over land, the surface heats up during the day as the excess heat is removed by moist convection. As the land and air temperatures equalize in the evening to the convection transition temperature, convection essentially stops and the land cools more slowly at night by net LWIR emission through the atmospheric LWIR transmission window. The convection transition temperature is reset each day by the local weather system passing through. Over the oceans, the surface temperature must increase until the water vapor pressure at the surface is sufficient to dissipate the excess heat by wind driven evaporation. A maximum ocean warm pool surface temperature near 30 C is needed to dissipate the tropical solar flux at an average wind speed near 5 m s^{-1}.

Over the last 200 years, the atmospheric concentration of CO_2 has increased by about 120 ppm from 280 to 400 ppm. This has produced an increase of approximately 2 W m^{-2} in the downward LWIR flux from CO_2 reaching the surface. When this increase in LWIR flux is coupled dynamically to the surface flux balance, the change in surface temperature is too small to measure.

References

Arrhenius, S., Philos. Trans. **41** 237-276 (1896), 'On the influence of carbonic acid in the air upon the temperature of the ground'

Clark, R. 2019a, '*A Dynamic Coupled Thermal Reservoir Approach to Atmospheric Energy Transfer Part III: The surface Temperature*', Ventura Photonics Monograph, VPM 004.1, Thousand Oaks, CA, May 2019

http://venturaphotonics.com/files/CoupledThermalReservoir_Part_III_Surface_Temperature.pdf

Clark, R. 2019b, '*A Dynamic Coupled Thermal Reservoir Approach to Atmospheric Energy Transfer Part IV: The Null Hypothesis for CO_2*' Ventura Photonics Monograph, VPM 005.1, Thousand Oaks, CA, May 2019

http://venturaphotonics.com/files/CoupledThermalReservoir_Part_IV_The_Null_Hypothesis.pdf

Clark, R. 2019c, '*A Dynamic Coupled Thermal Reservoir Approach to Atmospheric Energy Transfer Part V: Summary*', Ventura Photonics Monograph, VPM 006, Thousand Oaks, CA, May 2019

http://venturaphotonics.com/files/CoupledThermalReservoir_Part_V_Summary.pdf

Clark, R. 2019d, '*The Greenhouse Effect*', Ventura Photonics Monograph, VPM 003.2, Thousand Oaks, CA, May 2019

http://venturaphotonics.com/files/The_Greenhouse_Effect.pdf

Clark, R., 2013a, Energy and Environment **24**(3, 4) 319-340 (2013), 'A dynamic coupled thermal reservoir approach to atmospheric energy transfer Part I: Concepts'

http://venturaphotonics.com/files/CoupledThermalReservoir_Part_I_E_EDraft.pdf

Clark, R., 2013b, Energy and Environment **24**(3, 4) 341-359 (2013) 'A dynamic coupled thermal reservoir approach to atmospheric energy transfer Part II: Applications'

http://venturaphotonics.com/files/CoupledThermalReservoir_Part_II__E_EDraft.pdf

Clark, R., 2011, *The dynamic greenhouse effect and the climate averaging paradox*, Ventura Photonics Monograph, VPM 001, Thousand Oaks, CA, Amazon, 2011.
https://www.amazon.com/Dynamic-Greenhouse-Climate-Averaging-Paradox/dp/1466359188/ref=sr_1_1?s=books&ie=UTF8&qid=1318571038&sr=1-1

ENSO Index, 2018, ftp://www.coaps.fsu.edu/pub/JMA_SST_Index/jmasst1868-today.filter-5

Feldman D.R., Liou K.N., Shia R.L. and Yung Y.L., J. Geophys Res. **113** D1118 pp1-14 (2008), 'On the information content of the thermal IR cooling rate profile from satellite instrument measurements'

Harde, H., Int. J. Atmos. Sci.9251034 (2017), 'Radiation Transfer Calculations and Assessment of Global Warming by CO_2' https://doi.org/10.1155/2017/9251034

Keeling, R., http://scrippsco2.ucsd.edu/data/atmospheric_co2/primary_mlo_co2_record

Loeb, N. G.; B. A. Wielicki, D. R. Doelling, G. L. Smith, D. F. Keyes, S. Kato, N. Manalo-Smith and T. Wong, Journal of Climate **22**(3) 748-766 (2009), 'Toward Optimal Closure of the Earth's Top-of-Atmosphere Radiation Budget'.

Manabe, S. and R. T. Wetherald, J. Atmos. Sci., **24** 241-249 (1967), 'Thermal equilibrium of the atmosphere with a given distribution of relative humidity'

http://www.gfdl.noaa.gov/bibliography/related_files/sm6701.pdf

Mengelkamp, H-T.; F. Beyrich, G. Heinemann, F. Ament, J. Bange, F. Berger, J. Bosenberg, T. Foken, B. Hennemuth, C. Heret, S. Huneke, Kp-P. Johnsen, M. Kerschgens, W. Kohsiek, J-P

Leps, C. Liebethal, H. Lohse, M. Mauder, W. Meijninger, S. Raasch, C. Simmer, T, Spiess, A. Tettebrand, J. Uhlenbrock and P. Zittel, Bull. Amer. Met. Soc. **87**(6) 775-786 (2006), 'Evaporation over a heterogeneous land surface'

MODTRAN 2018, http://forecast.uchicago.edu/Projects/modtran.orig.html

Muller, R. A.; J. Curry, D. Groom, R. Jacobsen, S. Perlmutter, R. Rohde, A. Rosenfeld, C. Wickham & J. Wurtele, J. Geophys. Res. **118** 5280-5286 (2013), 'Decadal variations in the global atmospheric land temperatures,'

http://static.berkeleyearth.org/pdf/berkeley-earth-decadal-variations.pdf

NOAA, TAO, 2012 TRITON buoy data http://www.pmel.noaa.gov/tao/data_deliv/deliv.html

Oke T. R., WMO/TD-No. 1250, World Meteorological Association, 2006, '*Initial guidance to obtain representative meteorological observations at urban sites*'

Sahlee, E.; A-S Smedman, A. Rutgersson, and H. Ulf, Journal of Climate **21**(22) 5925-5941 (2008), 'Influence of a New Turbulence Regime on the Global Air–Sea Heat Fluxes'

Sea Temperatures, 2018, https://www.seatemperature.org/north-america/

SOI Index, 2018, ftp://ftp.bom.gov.au/anon/home/ncc/www/sco/soi/soiplaintext.html

Taylor, F. W., *Elementary Climate Physics*, Oxford University Press, Oxford, 2006, Chapter 7

Yu, L., J. Climate, **20**(21) 5376-5390 (2007), 'Global variations in oceanic evaporation (1958-2005): The role of the changing wind speed'

Yu, L., Jin, X. and Weller R. A., *OAFlux Project Technical Report* (OA-2008-01) Jan 2008, 'Multidecade Global Flux Datasets from the Objectively Analyzed Air-sea Fluxes (OAFlux) Project: Latent and Sensible Heat Fluxes, Ocean Evaporation, and Related Surface Meteorological Variables' http://oaflux.whoi.edu/publications.html

Volokin, D. and L. ReLlez, SpringerPlus, 3:723 pp 1-21 (2014), 'On the average temperature of airless spherical bodies and the magnitude of Earth's atmospheric thermal effect' https://springerplus.springeropen.com/articles/10.1186/2193-1801-3-723

Wilson, R. C., Astrophys Space Sci DOI 10.1007/s10509-014-1961-4, pp 1-14 (2014), 'ACRIM3 and the Total Solar Irradiance database'

http://web.b.ebscohost.com/ehost/pdfviewer/pdfviewer?vid=1&sid=7aa345a1-508d-4fd3-89c3-8818cf88d3b1%40pdc-v-sessmgr05